Journal of Medicinal Chemistry

Targeting Tyrosinase: Development and Structural Insights of Novel Inhibitors Bearing an Arylpiperidine/Arylpiperazine Fragment

Stefania Ferro, Batel Deri, Maria Paola Germanò, Rosaria Gitto, Laura Ielo, Maria Rosa Buemi, Giovanna Certo, Serena Vittorio, Antonio Rapisarda, Yael Pazy, Ayelet Fishman, and Laura De Luca

J. Med. Chem., **Just Accepted Manuscript** • DOI: 10.1021/acs.jmedchem.7b01745 • Publication Date (Web): 10 Apr 2018

ACS Publications

is published by the American Chemical Society. 1155 Sixteenth Street N.W., Washington, DC 20036

Targeting Tyrosinase: Development and Structural Insights of Novel Inhibitors Bearing an Arylpiperidine/Arylpiperazine Fragment

Stefania Ferro[a,∞], *Batel Deri,*[b, ∞] *Maria Paola Germanò*[a], *Rosaria Gitto*[a], *Laura Ielo*[a], *Maria Rosa Buemi*[a], *Giovanna Certo*[c], *Serena Vittorio*[a,c], *Antonio Rapisarda*[a], *Yael Pazy*[d], *Ayelet Fishman*[b], *Laura De Luca*[a,]*

[a] Dipartimento di Scienze Chimiche, Biologiche, Farmaceutiche e Ambientali (CHIBIOFARAM) Polo Universitario SS. Annunziata, Università di Messina, Viale Annunziata I-98168 Messina, Italy

[b]Department of Biotechnology and Food Engineering, Technion-Israel Institute of Technology, Haifa, 3200003, Israel

[c]Fondazione Prof. Antonio Imbesi, Piazza Pugliatti 1, 98100 Messina, Italy

[d]Technion Center for Structural Biology, Technion-Israel Institute of Technology, Haifa, 3200003, Israel

∞S.F. and B.D. contributed equally to this work.

KEYWORDS Tyrosinase, microwave irradiations, X-ray crystallography, docking studies, Ty Inhibitors

ABSTRACT

Inhibition of tyrosinase (Tys, EC 1.14.18.1) represents an efficient strategy to decrease melanogenesis and skin hyperpigmentation. A combination of crystallographic and docking studies on two different tyrosinase, from *Bacillus megaterium (TyBm)* and from mushroom *(TyM)* has contributed to increase our knowledge about their structural information and translating them on the most druggable human Ty (TyH) isozyme. In particular we designed and synthesized a series of 1-(4-fluorobenzyl)piperazine and 1-(4-fluorobenzyl)piperidine derivatives showing inhibitory activity on TyM at micromolar range resulting more potent than reference compound kojic acid. The crystal structures of TyBm with inhibitor **3 (**IC_{50} value of 25.11 μM**)** and **16 (**IC_{50} value of 2.03 μM) were solved confirming the binding pose hypothesized by *in silico* studies and revealing the main molecular determinants for the binding recognition of the inhibitors.

INTRODUCTION

Tyrosinases (Tys, EC 1.14.18.1) are metalloenzymes abundant in a wide range of organisms (mammals, fungi, bacteria and plants). Tys display a binuclear active site, composed by two copper ions coordinated by six histidine residues, and catalyze the oxidation of phenols and catechols into catechols and *ortho*-quinones, respectively. In mammals, the conversion of L-tyrosine into quinones is considered the key step of melanogenesis in which generated melanin pigments play an important role in prevention of skin damage due to UV radiation and free radicals.[1, 2] It is well-known that melanin-related pathologies can cause skin hyperpigmentation, lesions or melasma.[3] Thus, Ty inhibition is one strategy aimed at controlling the production of melanin. Consequently, the development of Ty inhibitors (TyIs) gained high interest in the therapy of skin pathologies as well as in dermocosmetic treatments. Several TyIs such as hydroquinone, arbutin or kojic acid are currently used as depigmentation agents.[4] Unfortunately, these inhibitors demonstrated relevant

human toxicity.[3] There are different Ty enzymes from distinct sources such as human (TyH), mushroom (*Agaricus bisporus*, TyM) and bacterial (e.g. *Bacillus megaterium*, TyBm) that share low similarity around 10–30%.[5] Both TyM and TyBm are cytosolic proteins, whereas TyH is a monomeric glycosylated transmembrane isoform. Probably due to the different architecture of these isozymes, some effective inhibitors of TyH revealed poor activity against TyM and vice versa.[6]

No structural data is currently available for the most druggable TyH at atomic resolution, with exception of homology models built with TyBm and *Ipomea batata* cathecol oxidase[7] and the recently reported structure of tyrosinase related protein 1.[8] On the contrary structural and biochemical information has been reported for TyM and TyBm.

To start our exploration we focused our studies on the available TyM and TyBm which share 58% identity within 6 Å from the two copper centers[5, 9] to obtain molecular probes for the identification of selective Ty inhibitors. To evaluate the inhibitory activity of our designed derivatives we followed the most employed Ty inhibition assay protocol which apply TyM that consequently is used as protein structure for our docking studies. To gain more strength at our computational results we performed[10] the crystal studies of our ligands with the TyBm which share an higher homology with to the human enzyme.

It has been reported that compounds from natural or synthetic sources (chalcones, flavonoids, coumarins, thioureas, peptides, and so on) can affect the Ty active site as substrates, competitive, and non-competitive inhibitors.[4] The distinct mode of action is dependent on their different chemical moieties which mimic the phenol/catechol group of the natural substrates L-tyrosine or L-DOPA.

We have previously discovered small compounds from synthetic sources as a new class of TyM inhibitors and some of them displayed higher efficacy than reference compound kojic acid.[11, 12] Specifically, the most active inhibitor was the 1-(5,6-dimethoxy-1*H*-indol-3-yl)-2-(4-(4-fluorobenzyl)piperidin-1-yl)propan-1-one (**1**, **Figure 1**) that demonstrated promising inhibitory effects (IC_{50} value of 7.56 μM) affecting diphenolase activity as a mixed-type inhibitor.[12] Our

structure-affinity relationship (SAR) studies highlight that the 4'-fluorobenzyl moiety embedded in the 4-position of piperidine fragment was present in the most active inhibitors, thus suggesting a plausible crucial role in controlling inhibitory effects toward TyM. This SAR analysis was consistent with our preliminary X-ray studies of co-crystal structure of inhibitor **1** in complex with TyBm.[12] Specifically, the electron density observed in the active site of TyBm confirmed that the 4'-fluorobenzyl moiety of compound **1** is situated between the two copper ions, with the aromatic ring stabilized through stacking interactions with residue His208 (**Figure 1**).

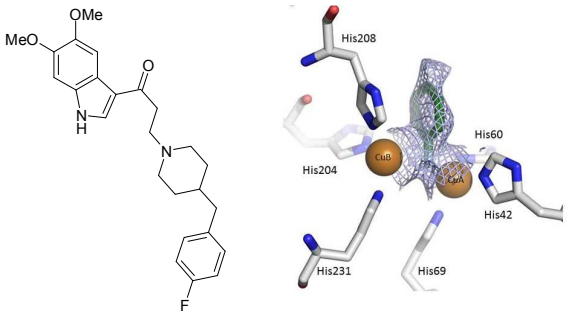

Figure 1. Chemical structure of 1-(5,6-dimethoxy-1H-indol-3-yl)-2-(4-(4-fluorobenzyl)piperidin-1-yl)propan-1-one (**1**) and co-crystal structure of the 4-fluorobenzyl portion of inhibitor **1** and TyBm.[12]

As the substrate was not fully visualized,[12] this structure was not deposited in the protein data bank but presented a good starting point for the development of a further series of compounds. On this basis we herein designed new inhibitors bearing a 4'-fluorobenzyl moiety as a crucial structural requirement for the recognition of TyIs in the catalytic site. All compounds were generally prepared by means of microwave-assisted organic synthetic approaches. For this new class of TyIs, SAR has been investigated by combining theoretical, experimental and structural information.

RESULTS AND DISCUSSION

To identify new TyIs we began a rational design process through *in silico* studies starting from the smallest active inhibitor previously identified in our research work, namely 1-ethyl-4-[(4-

fluorophenyl)methyl]piperidine derivative (**2**, **Figure 2**). Specifically, for this compound the inhibition of TyM diphenolase activity in presence of L-DOPA as a substrate resulted in an IC_{50} value of 116 μM.[12] We performed docking studies by GOLD software[13] and investigated the binding pose of compound **2** in the active site of TyM from *Agaricus bisporus* retrieved from Protein Data Bank (PDB code 2Y9X). Considering the high flexibility of prototype **2**, we have applied the "scaffold match constraint approach" for the 4-fluorophenyl moiety to close-in its binding pose based on the co-crystal structure of the active portion of inhibitor **1** (**Figure 2**).

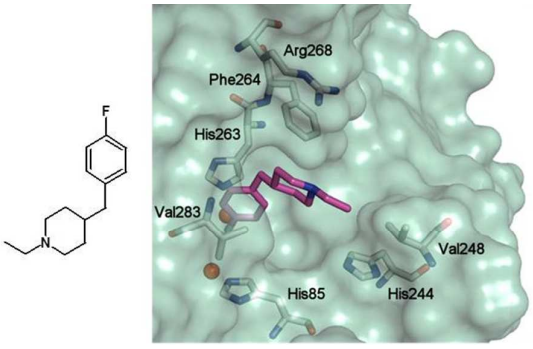

Figure 2. Chemical structure of 1-ethyl-4-[(4-fluorophenyl)methyl]piperidine derivative (**2**) and proposed binding mode in the active site of TyM from *Agaricus bisporus* (PDB code 2Y9X).

Apart from the expected key π–π stacking interactions between His263 (His208 in TyBm, **Figure 1**) and the 4'-fluorophenyl ring, the N-ethylpiperidine portion of compound **2** seems to engage profitable contacts with the hydrophobic area defined by residues Val248, Phe264, and Val283 (**Figure 2**). Moreover, the visual inspection of docking pose of compound **2** suggests that close to the N-ethyl substituent there is a wide pocket which might be an amenable area to further investigate SARs for this class of compounds. In the first round of our novel study we designed a small series of analogs of compound **2** bearing N-acyl moieties. We introduced new functionalities to exploit additional hydrophilic/hydrophobic interactions with residues paving the large entrance of the catalytic site pocket. The first designed compound was the 1-(4-(4'-fluorobenzyl)piperidin-1-yl)ethanone (**3**), that could assume a very similar binding pose of inhibitor **2** within the TyM

catalytic pocket. Thus compound **3** was readily obtained by acetylation of commercially available 4-(4-fluorobenzyl)piperidine (**4**) (**Scheme 1**).

Scheme 1.

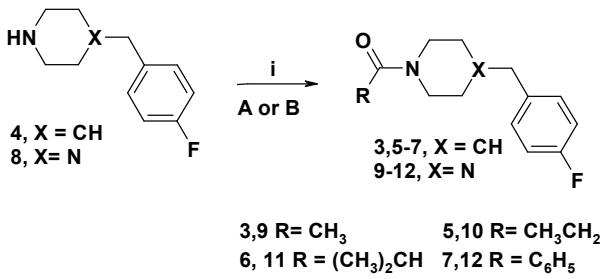

Reagents and conditions: i) Appropriate acyl chloride: Pathway A: TEA, THF, 0°C, rt, 10 min; Pathway B: DMF, K_2CO_3, MW 5 min, 100°C, 200 W.

To start with SAR exploration, we also chose to replace the acetyl group with other bulky substituents able to make favorable hydrophobic interactions in the surrounding area defined by the residues reported above. As described in **Scheme 1** we have synthesized a small series of homologues of amide **3** such as the propionamide-, isobutyramide- and benzamide derivatives **5**, **6** and **7**. In the second round of our structural modifications we decided to change the central piperidine core with a piperazine one. Specifically, we selected the piperazine linker on the basis of the measured inhibitory properties of 1-(4-fluorobenzyl)piperazine (**8**) fragment, which resulted in about 3-fold higher inhibition than 4-(4-fluorobenzyl)piperidine (**4**) against diphenolase activity of TyM (IC_{50} = 85.5 μM *versus* 286.83 μM). As shown in Scheme 1 we have synthesized the designed amide derivatives **9-12** as piperazine analogs of amides **5-7**. For compound **9** the reaction was carried out at room temperature in the presence of TEA (pathway A). Whereas, the amides **10-12** were readily obtained by applying microwave irradiations in alkaline medium (pathway B).[14]

All of the new synthesized compounds **3**, **5-7**, **9-12** were initially tested as inhibitors of TyM against diphenolase activity and the results are summarized in **Table 1**.

It was interesting to note that the newly designed amide **3** (IC_{50} = 25.11 μM) displayed about five-fold improvement of inhibitory properties when compared with the previously synthesized amine **2**. In addition, homologous amides **5-7** demonstrated similar potency to the parent compound **3**. Among the series of piperazine-based amides **9-12**, the most active inhibitor was the (4-(4-fluorobenzyl)piperazin-1-yl)(phenyl)methanone **12** (R = Ph, IC_{50} = 13.3 μM) thus suggesting that the combination of the N-benzoyl substituent with the piperazine core induced an improvement in inhibitory effects.

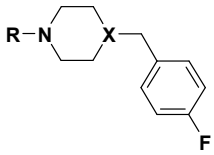

Table 1. TyM inhibition of target compounds **2-12** and Kojic acid.

	R	X	IC_{50}[a] (μM)
2[b]	CH_3CH_2	CH	116.0 ± 1.88
3	CH_3CO	CH	25.11 ± 0.98
4[b]	H	CH	286.83 ± 1.05
5	CH_3CH_2CO	CH	24.10 ± 0.62
6	$CH_3CH(CH_3)CO$	CH	35.26 ± 0.97
7	C_6H_5CO	CH	19.50 ± 0.44
8	H	N	85.50 ± 0.67
9	CH_3CO	N	45.85 ± 1.31
10	CH_3CH_2CO	N	51.08 ± 4.88
11	$CH_3CH(CH_3)CO$	N	30.90 ± 1.90
12	C_6H_5CO	N	13.34 ± 0.73
Kojic acid			17.76 ± 0.18

[a]All compounds were examined in a set of experiments performed in three replicates with L-DOPA as the substrate; IC_{50} values represent the concentration that caused 50% enzyme activity loss. [b]Data taken from ref. 12.

In order to understand the intricate binding mode of this first series of amides **3, 5-7, 9-12**, we tried to obtain crystal complexes of these compounds with TyBm. The crystal structure was obtained only for amide **3** in the active site of TyBm at 2.7Å resolution (**Figure 3A**, **Table 2** and Supplementary **Figure S1**).

The 4-fluorobenzyl moiety of amide **3** is oriented towards CuA at a distance of 1.9Å and is stabilized by hydrophobic π-π interactions with His208. In addition, a hydrogen bond is observed between Arg-209 and the oxygen atom of the carbonyl group of amide **3** (Figure 3B), similarly to tyrosinase substrates, tyrosine and L-DOPA, reported by Goldfeder et al.[15] The binding pocket of TyBm shows high similarity with the TyM structure[16] and therefore it is hypothesized that the additional bonds made by the carbonyl group of amide **3** may contribute to improve the TyM affinity when compared to amines **2** and **4** (**Table 1**). Moreover, the orientation of amide **3** in the active site of TyBm is similar to the recently determined structures with kojic acid and hydroquinone,[17] as well as docking studies with novel biphenyl ester derivatives,[18] supporting the role of this compound as a tyrosinase inhibitor. Comparing the positioning of bound amide **3** and kojic acid (KA, PDB 5I38), one major difference observed is the movement of Arg209 (Figure 3C). The flexibility of Arg209 has been reported beforehand for TyBm,[19] it facilitates the stabilization of ligands in the active site resulting in higher inhibition by amide **3**.

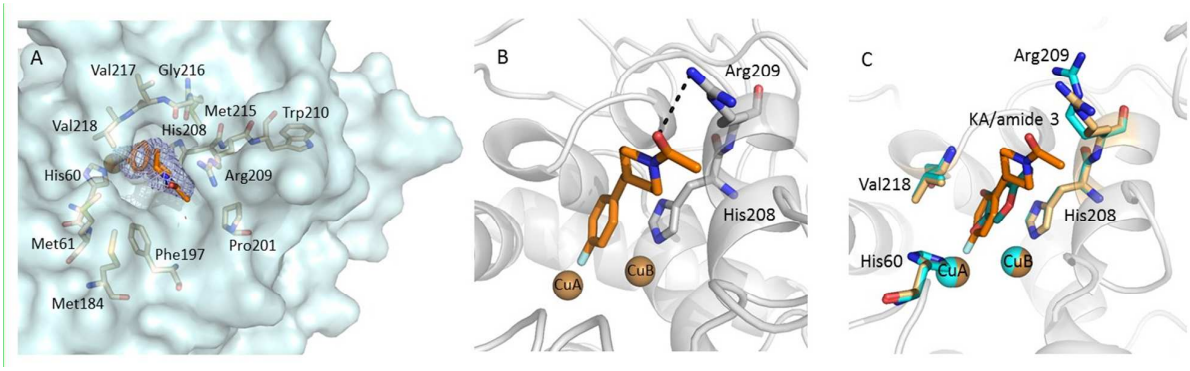

Figure 3: Structures of 1-(4-(4-fluorobenzyl)piperidin-1-yl)ethanone (**3**) bound in the active site of tyrosinase from *Bacillus megaterium* (TyBm) (PDB 5OAE). A) Amide **3** (orange) is observed in the active site of TyBm (cyan surface) with its mFO-DFC electron density polder map (blue wire) contoured at 3σ. Copper ions are presented as brown spheres and residues surrounding the active site are in light blue sticks. B) Amide **3** (orange) positioned in the active site of TyBm with the oxygen atom of the carbonyl group forming a hydrogen bond with Arg209. C) Superposition with

TyBm structure binding kojic acid (cyan, PDB 5I38). Kojic acid (deep teal) and amide **3** (orange) are oriented through hydrophobic interactions with His208. Copper ions, residues Val218 and His60 are identical, whereas Arg209 moves. All the structures presented were generated using PyMOL.[20]

To better compare this structural information with biochemical results, we attempted to determine the IC_{50} values of amide **3** with TyBm, however inhibition was not detected due to the poor solubility of derivative in buffer, necessitating the use of DMSO as a co-solvent in biochemical experiments. Control experiments with DMSO alone resulted in activation of TyBm explaining the lack of inhibition in the tested conditions. DMSO possibly affects the movement of Arg209 in the active site of TyBm as was reported previously for SDS and ionic liquids. SDS levels of 2–50 mM increased the activity of TyBm by 2-fold towards the natural substrates L-tyrosine and L-Dopa and 15- to 20-fold towards phenol and catechol.[19] Kojic acid, which is soluble in water, inhibited TyBm with an IC_{50} value of 52 μM,[17] quite similar to the value obtained with TyM (17.76 μM, **Table 1**, experimental conditions were not identical) confirming the assumption that in the absence of an organic solvent, compound **3** might inhibit TyBm.

Table 2. Data collection and refinement statistics

Structure name (PDB code)	TyBm:**3** (5OAE)
Data collection	
Space group	$P2_12_12_1$
Cell dimensions	
a, b, c (Å)	78.45,84.10, 89.76
α, β, γ (°)	90, 90, 90
Resolution (Å)	39.59-2.7
*R*merge[*,†]	0.11(0.71)
$I/\sigma I$[*]	10.9(2.6)
Completeness[*]	92.0(95.6)
Redundancy[*]	3.9(4.1)
Refinement	
Resolution (Å)	38.96-2.7
Total reflections	59333(9330)

Unique reflections	15340(2286)
*R*work/*R*free‡	21.64/26.09
No. of atoms	
Protein	4,699
Ligand/ion	38
Water	44
B-factors (Å)	
Protein	42.30
Ligand/ion	52.60
Water	40.90
Root mean square deviations	
Bond length (Å)	0.003
Bond angle (°)	0.731

*Values in parentheses are for the last shell.†$R_{merge}= \sum_{hkl}\sum_i |I_i(hkl)-\langle I(hkl)\rangle|/ \sum_{hkl}\sum_i I_i(hkl)$, where *I* is the observed intensity, and <*I*> is the mean value of *I*. ‡$R/R_{free} = \sum_{hkl}||F_{obs}| - |F_{calc}||/\sum_{hkl}|F_{obs}|$ where *R* and R_{free} are calculated using the test reflections respectively. The test reflections (5%) were held aside and not used during the entire refinement process.

To gain further insights into the binding mode of inhibitor **3** in the catalytic site of TyM, docking analysis was performed (**Figure 4A**). We applied appropriate flexibility to the side chains of the protein during docking simulations revealing that the 1-(4-fluorobenzyl) fragment establishes π-π interactions with His263 at the active site, while the oxygen atom of carbonyl group of **3** creates a polar contact with Arg268 similar to the hydrogen bond found for Arg209 in the adduct TyBm/**3** (**Figure 3B**).

Overall, these studies suggest that the docking pose of amide **3** (Figure 4A) in TyM is consistent with the binding orientation of inhibitor **3** in complex with TyBm. This observation sustains the reliability of our docking simulations in analyzing the interactions with TyM of all tested compounds as reported for the best active inhibitor **12** displayed in **Figure 4B**.

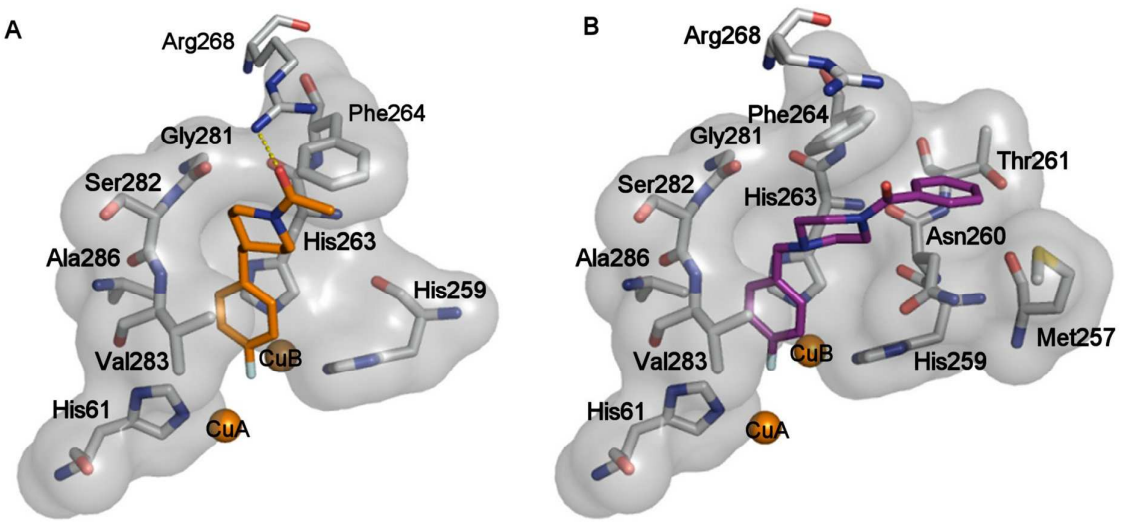

Figure 4: Suggested binding mode of compounds **3 (A)** (yellow) and **12 (B)** (purple) that were docked into the TyM strcuture (PDB code 2Y9X). Key residues of the pocket are presented and hydrogen bond interactions are showed by dotted lines. The interactions between the TyM and inhibitors **3** and **12** were examined using PyMOL[20] and LIGPLUS.[21] The figure was created using PyMOL software.[20]

The docking simulation of active benzamide **12** suggests that the 1-(4-fluorobenzyl) fragment maintains a very similar orientation; whereas the benzoyl portion is oriented towards an exposed region located at the entrance of catalytic area (**Figure 4, panel B**). In particular, the aromatic ring occupies the area paved by amino acid residues Met257, Asn260, Thr261 and Phe264 lining both hydrophobic and hydrophilic regions. By comparing the docking pose of active inhibitors **3** and **12,** we have hypothesized that the profitable hydrogen bond contact with Arg268 of acetamide **3** was replaced by hydrophobic interactions produced by the phenyl ring of benzamide **12** and the two residues Met257 and Phe264. Therefore, in absence of H-bond interaction with Arg268 these additional interactions could keep the inhibitor **12** in a good orientation in the catalytic pocket.

Based on these insights for benzamide **12**, we designed new derivatives that bear additional substituents in *ortho*, *meta* and *para* position of the phenyl ring. Our idea was to probe further hydrophobic/hydrophilic contacts that might increase the interaction in the cavity occupied by the benzoyl fragment. We initially selected the following substituents: fluorine atom and methyl, methoxy, hydroxyl groups, thus exploring the role of the hydrophobic and electronic nature of the

substituents. This small series of twelve aroylpiperazine derivatives **13-24** was obtained by coupling the 1-(4-fluorobenzyl)piperazine (**8**) with a suitable aroylchlorides resulting in the corresponding amides **13-21** in good yields. In turn, the alkoxy derivatives **19-21** were converted to the corresponding hydroxyl derivatives **22-24** by treatment with boron tribromide.

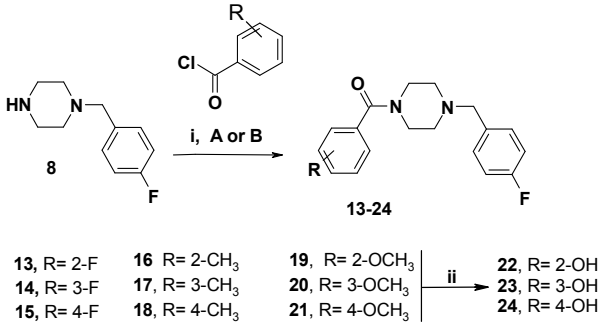

Scheme 2: Reagents and conditions: i) Pathway A: R=2-OCH_3, R=3-OCH_3, R=4-OCH_3, DCM, EDIPA, r.t, 5h; pathway B: R=2-F, R=3-F, R=4-F, R=2-CH_3, R=3-CH_3, R=4-CH_3, DCM, EDIPA, MW: 10 min, 50°C, 200W; ii) BBr3, DCM, 0°C, r.t., 24h.

Table 3 summarizes the results of biochemical screening of benzamides **13-24** for which we generally obtained a significant improvement of inhibitory activity with respect to the first series of tested compounds. Specifically, the most active inhibitor was compound **19** (R=2-OCH_3) which was up to 6-fold more potent than unsubstituted benzamide analog **12** (R=H) and more potent than the reference compound kojic acid (see **Table 1**). By modifying the 2-methoxysubstituent with other electron donating groups (EDG) such as methyl or hydroxyl groups, we found that both the obtained compounds **16** and **22** maintained high inhibitory effects.

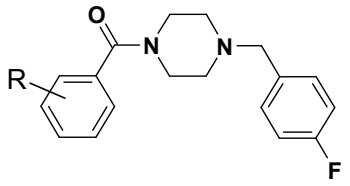

Table 3. TyM inhibition of target compounds **13-24**

	R	IC_{50}[a]
13	2-F	3.75 ± 0.37 μM
14	3-F	54.68 ± 6.03 μM

15	4-F	7.77±2.89 μM
16	2-CH_3	5.25±1.60 μM
17	3-CH_3	173.82±1.5 μM
18	4-CH_3	33.13±4.50 μM
19	2-OCH_3	2.03±0.89 μM
20	3-OCH_3	27.04±0.05 μM
21	4-OCH_3	9.14±2.16 μM
22	2-OH	7.06±0.62 μM
23	3-OH	12.64±1.41 μM
24	4-OH	27.41±0.16 μM

[a]All compounds were examined in a set of experiments performed in three replicates; IC_{50} values represent the concentration that caused 50% enzyme activity loss.

It was interesting to note that the switch of methyl/methoxy/hydroxy substituent to the *meta* or *para* position generally led to less active inhibitors. Specifically, the most significant reduction of inhibitory effect was found for the meta-substituted compound **17** that resulted in 35-fold lower IC_{50} compared to the *ortho*-substituted analog **16.** The presence of a fluorine atom as a small electron withdrawing group (EWG) resulted in improvement of affinity when compared with the unsubstituted analog **12**.

Furthermore, the inhibition kinetics of the most promising inhibitor **19** (IC_{50} = 2.03 μM), on the diphenolase activity of mushroom tyrosinase were studied using Lineweaver-Burk double reciprocal plots (see **Figure 5**). The results showed that the plots of 1/V versus 1/[S] gave straight lines with different slopes intersecting the horizontal axis. These data suggest that compound **19** acts as a non-competitive inhibitor since it is able to bind with equal affinity to the free enzyme as well as to the enzyme-substrate complex. The increase in concentrations of **19** corresponds to the decrease of V_{max} values, while K_m values remain unchanged. Therefore, it is assumed that the inhibitor might occupy the active site as well as hinder the access of substrate L-DOPA.[22, 23]

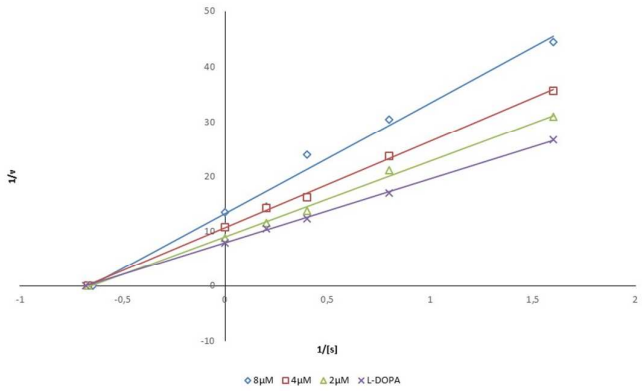

Figure 5: Lineweaver-Burk plots for the inhibition of mushroom tyrosinase respect to L-DOPA as substrate in the presence of the best active inhibitor **19.**

To simulate the binding recognition into the enzymatic cavity we docked the best active inhibitor **19** (blue) into the TyM structure (PDB code 2Y9X) and compared its pose with the binding pose of parent compound **12** (purple) (**Figure 6**). As expected, the two inhibitors were almost superimposable thus sharing very similar molecular interactions. Notably, the 2-methoxy-substituent of the best active compound **19** is projected towards residue Val248 thus making an additional hydrophobic interaction. Overall, the proposed binding mode for the best active ligand **19** was in good agreement with our biochemical assays for which **19** displayed non-competitive inhibition of TyM.

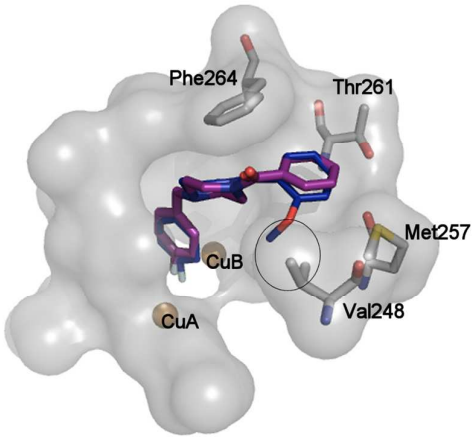

Figure 6. Alignment of the binding poses of benzamides **12** (purple) and **19** (blue) that were docked into the TyM (PDB code 2Y9X). The circle highlights the contact between methyl group and Val248 in the hydrophobic region of the cavity. Copper ions are depicted in brown. The figure was created using PyMOL software[20]

The positioning found out for compound **19** in the active site of TyM (**Figure 6**) might lead to the false assumption of a competitive inhibition mechanism. However, we suggest that it could also bind to a peripheral binding site in TyM yet to be elucidated. It was previously shown by Deri *et al*. [17] that KA binds in two regions within the enzyme, inside the active site and at the entrance to the active site, giving rise to mixed inhibition kinetics. These results were demonstrated by crystallography as well as by *in silico* simulations. In addition, tropolone, another well-known tyrosinase inhibitor, was also found at the active site entrance of TyM and exhibited mixed inhibition mode.[22] It is assumed that this additional binding mode of compound **19** in the peripheral site of TyM could restrict substrate entrance and product efflux, consequently, the non-competitive inhibition mode is obtained kinetically (see **Figure 5**).

In order to gain more molecular insights on the binding mode of designed benzamide derivatives, attempts were carried out to obtain co-crystal complexes with TyBm. A further structure was successfully determined for compound **16** in the active site of TyBm at 2.0Å resolution (**Figure 7, Table 4** and Supplementary Figure S2). As expected, the 4-fluorobenzyl moiety of derivative **16** is oriented towards CuA and is stabilized through stacking interactions with His208. In addition, a polar interaction between benzamide **16** and Arg209 is observed, similar to the orientation of compound **3** in TyBm active site (**Figure 7**). Comparing the positioning of bound amide **3** and benzamide **16**, the major difference observed is the slight movement of Arg209 (**Figure 7B**). The mobility of Arg209 allows the stabilization of bulky compounds in the active site of TyBm.

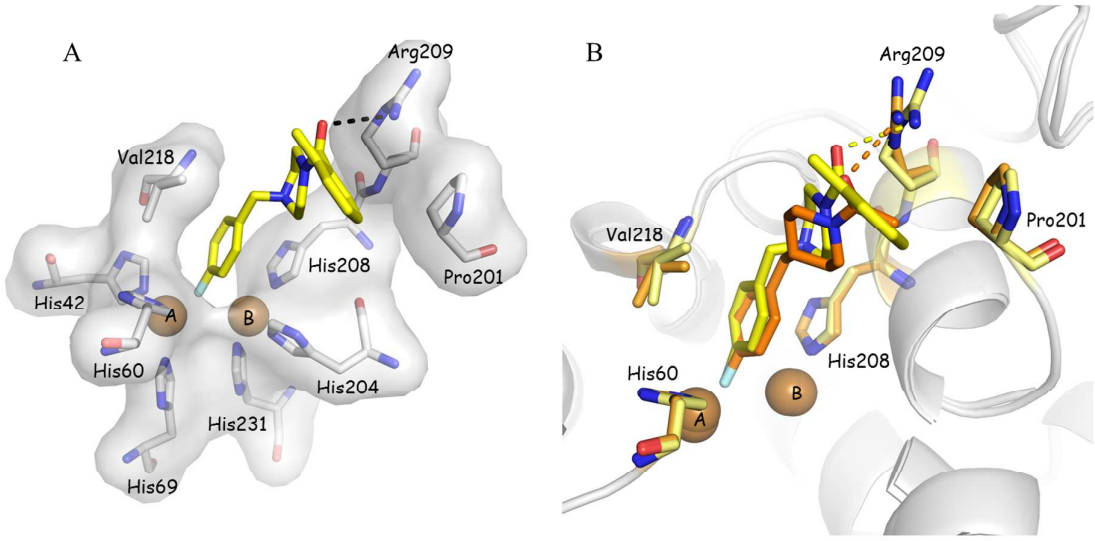

Figure 7. Structure of benzamide **16** bound in the active site of TyBm. (A) Benzamide **16** (yellow) positioned in the active site of TyBm with the oxygen atom of the carbonyl group forming a hydrogen bond with Arg209. (B) Superposition with bound amide **3** (orange). Copper ions are presented as brown spheres.

Table 2. Data collection and refinement statistics

Structure name (PDB code)	TyBm:**16** (6EI4)
Data collection	
Space group	$P2_1$
Cell dimensions	
a, b, c (Å)	53.65,78.10, 81.05
α, β, γ (°)	90, 104.52, 90
Resolution (Å)	28.10-1.69
*R*merge*,†	0.13(0.48)
$I/\sigma I$*	6.5(3.1)
Completeness*	98.8(98.4)
Redundancy*	5.2(5.4)
Refinement	
Resolution (Å)	28.10-2.0
Total reflections	375111(55945)
Unique reflections	71968(10437)
*R*work/*R*free‡	22.01/24.75
No. of atoms	
Protein	4,719
Ligand/ion	50
Water	358

B-factors (Å)	
Protein	27.74
Ligand/ion	41.75
Water	27.54
Root mean square deviations	
Bond length (Å)	0.008
Bond angle (°)	1.02

*Values in parentheses are for the last shell.†R_{merge}= $\sum_{hkl}\sum_i$ $|I_i(hkl)-\langle I(hkl)\rangle|/ \sum_{hkl}\sum_i I_i(hkl)$, where I is the observed intensity, and $<I>$ is the mean value of I. ‡R/R_{free} = $\sum_{hkl}||F_{obs}| - |F_{calc}||/\sum_{hkl}|F_{obs}|$ where R and R_{free} are calculated using the test reflections respectively. The test reflections (5%) were held aside and not used during the entire refinement process.

This additional structural information confirmed that the two inhibitors **3** and **16** share a very similar binding mode within catalytic site of TyBm. These experimental data were consistent with the suggested pose of inhibitor **16** docked in the catalytic site of TyM (Supplementary **Figure S3**) in comparison with analogues **12** and **19**. Considering that the inhibition kinetics suggest that the inhibitor **16** displays (Supplementary **Figure S4**) a mode of interaction similar to that we found for compound **19** (see **Figure 5**), we can speculate that both **16** and **19** could hamper the enzymatic activity of TyM through a singular mechanism of interaction that might involve additional and peripheral binding regions.

As there is currently no structure of the human enzyme, we finally decided to collect our acquired structural information for TyM and TyB and translate these achievements on the druggable TyH through the employment of TyH model and melanogenic protein TYRP1.

The active site of all tyrosinases is similar as demonstrated by the superposition of the TyH model with TyM and TyBm (Figure S5), including residues Asn205 and Glu195 (in TyBm) which are crucial for activity through the activation of a conserved water molecule.[24] Favre *et. al.* used quantum mechanics to model TyH and showed that their model, deposited in the Protein Model Database, is a reliable structure for future rational inhibitor design projects.[7] In addition, the crystal structure of human tyrosinase related protein 1 (TYRP1) was recently solved and revealed for the first time the structure of a mammalian tyrosinase family member. The TYRP1 structure contains a

tyrosinase-like subdomain that has the typical tyrosinase fold with a binuclear type 3 metal binding site. It is a zinc-binding enzyme which makes it unlikely to be a redox catalyst. However when exchanging the zinc cofactor to copper, a slight tyrosinase activity was detected.[8] Human TYRP1 was shown to be highly similar to TyBm with 32% sequence identity and an rmsd of 1.6Å for 263 aligned amino acids.[8] Furthermore, it was demonstrated that the catalytic domain with the active site is highly similar to that of type 3 copper proteins, especially to TyBm.[8, 24] Superposition of TyBm with bound kojic acid (PDB 5I38) and TYRP1 with bound kojic acid (PDB 5M8L) reveals similar orientation of the ligand towards CuA in both enzymes (**Figure S6**). Numerous reports exist on the IC_{50} values of TyH inhibition by ligands such as kojic acid and other natural products which inhibit TyM and TyBm with similar efficacy.[6, 25-28] Overall, it is well demonstrated in the literature that inhibitors of TyM and TyBm have relevance to the human enzyme and therefore the inhibitors developed here could have potential pharmaceutical implications. Clearly, more research is needed to confirm that the inhibitory effect of the most active derivatives might be moved to TyH.

CONCLUSIONS

To develop tyrosinase inhibitors as therapeutic agents for potential treatment of skin hyperpigmentation pathologies, we carried out the first "lead optimization" process which has been performed by combining X-ray crystallography and docking simulations within enzymatic cavity of TyBm and TyM isozymes. Specifically, theoretical and experimental structural determinations have been employed for the rational design of a small series of 1-(4-fluorobenzyl)piperazine and 1-(4-fluorobenzyl)piperidine derivatives. As a result, we have identified new inhibitors more potent than reference compound kojic acid (KA). The crystal structures of 1-(4-(4-fluorobenzyl)piperidin-1-yl)ethanone (**3**) and [4-(4-Fluorobenzyl)piperazin-1-yl](2-methylphenyl)methanone (**16**) in complex with TyBm revealed that the two inhibitors assume a similar binding pose of inhibitor KA in the enzyme catalytic cavity. Moreover, the co-crystal adducts highlighted a pivotal role of an additional H-bond contact between oxygen atom of carbonyl group with crucial residue Arg209 (TyBm) in the

rim of the catalytic cavity. The active inhibitors **16** and **19** displayed a non-competitive inhibition of TyM as supported by kinetic analysis. By means of docking simulations we have hypothesized that additional interactions with hydrophobic subpocket (Val248 and Met257, TyM) might be essential to improve the anchoring of inhibitors into binding site.

EXPERIMENTAL SECTION

Chemistry. All starting materials and reagents commercially available (Sigma-Aldrich Milan, Italy; Alfa Aesar Karlsruhe, Germany) were used without further purification. Microwave-assisted reactions were carried out in a focused Microwave Synthesis System (CEM Technology Ltd Buckingham, UK). Melting points were determined on a Buchi B-545 apparatus (BUCHI Labortechnik AG Flawil, Switzerland) and are uncorrected. Elemental analyses (C, H, N) were carried out on a Carlo Erba Model 1106 Elemental Analyzer (Carlo Erba Milano, Italy); the results confirmed a ≥95% purity. Merck silica gel 60 F254 plates were used for analytical TLC (Merck KGaA, Darmstadt, Germany). Flash Chromatography (FC) was carried out on a Biotage SP1 EXP (Biotage AB Uppsala, Sweden). ^{1}H NMR spectra were measured in $CDCl_3$ with a Gemini 300 spectrometer (Varian Inc. Palo Alto, California USA); chemical shifts are expressed in δ (ppm) and coupling constants (J) in Hz.

General Procedure to Synthesize Target Compounds 3, 5-7, 9-12 (Pathways A and B)

Pathway A: Acetyl chloride (2.05 mmol) was added to a solution of 1-(4-fluorobenzyl)piperazine (**8**) (2.05 mmol) in THF (7mL) and TEA (3.28 mmol). The mixture was stirred at room temperature for 10 min under nitrogen atmosphere. Then, the obtained precipitate was turned away by filtration and the solution was evaporated under reduced pressure to give the final compound **9** as crude product, which has been purified by chromatographic column (Cyclohexane/EtOAc 20:80). Pathway B: To prepare compounds **3, 5-7, 10-12** the suitable acyl chloride (1.5 mmol) was dissolved in DMF (1 mL). Then the 4-(4-fluorobenzyl)piperidine (**4**) or 1-(4-

fluorobenzyl)piperazine (**8**) (1.5 mmol) was added dropwise in the presence of K_2CO_3 (0.75 mmol). The reaction was carried out using microwave irradiations under the following conditions: 5 min, 100 °C. The mixture of reaction was quenched by addition of a saturated solution of $NaHCO_3$ (10 mL) and the aqueous phase was extracted with EtOAc (3x5 mL). The organic phase thus obtained was washed with brine (3x5mL) and dried with anhydrous Na_2SO_4. The solvent was removed under reduced pressure and the final products **3, 5-7, 10-12** were obtained after purification by chromatographic column (Cyclohexane/EtOAc 30:70).

The registered CAS numbers have been already assigned to compounds **3, 5-7, 9-12**. For these compounds the synthetic procedures, chemical properties and structural characterization are not available in literature, except for patented compounds **3**[29] and **7**[30].

1-[4-(4-Fluorobenzyl) piperidin-1-yl] propan-1-one (5). CAS Number: 1215411-97-4. Yield: 23%. Oily residue. ^{1}H-NMR ($CDCl_3$), (δ): 1.05-1.16 (m, 5H), 1.65-1.75 (m, 3H), 2.34 (q, 2H, CH_2), 2.50-2.53 (m, 3H), 2.93 (t, 1H, CH), 3.82 (m, 1H, CH_2), 4.61 (m, 1H, CH_2), 6.94-7.11 (m, 4H, ArH). Anal. Calcd for ($C_{15}H_{20}FNO$): C 72.26, H 8.09, N 5.62. Found: C 72.66, H 8.49, N 6.02.

1-[4-(4-Fluorobenzyl)piperidin-1-yl]-2-methylpropan-1-one (6). CAS Number: 1215420-69-1. Yield: 31%. Oily residue. ^{1}H-NMR ($CDCl_3$), (δ): 1.09-1.18 (m, 8H), 1.70 (m, 3H), 2.51 (m, 3H), 2.79-2.81 (m, 1H, CH) 2.96 (t, 1H, CH), 3.91 (m, 1H, CH_2), 4.63 (m, 1H, CH_2), 6.94-7.11 (m, 4H, ArH). Anal. Calcd for ($C_{16}H_{22}FNO$): C 72.97, H 8.42, N 5.32. Found: C 72.57, H 8.02, N 4.92.

1-[4-(4-Fluorobenzyl) piperazin-1-yl]ethanone (**9**) CAS Number: 415958-01-9.Yield: 20%. Oily residue. ^{1}H-NMR ($CDCl_3$), (δ): 2.09 (s, 3H, CH_3), 2.42 (m, 4H), 3.47 (m, 4H), 3.63-3.64 (m, 2H, CH_2), 7.00 (d, 2H, ArH, J= 8.8), 7.29 (d, 2H, ArH, J= 8.8). Anal. Calcd for ($C_{13}H_{17}FN_2O$): C 66.08, H 7.25, N 11.86. Found: C 66.48, H 7.65, N 12.26.

1-[4-[(4-Fluorophenyl)methyl]piperazin-1-yl]propan-1-one (10) CAS Number: 1328560-06-0. Yield: 33%. Oily residue. ^{1}H-NMR ($CDCl_3$), (δ): 1.14 (t, 3H, CH_3, J= 6.5, J= 6.4), 2.29-2.42 (m, 6H, CH_2), 3.43-3.48 (m, 4H, CH_2), 3.62-3.64 (m, 2H, CH_2), 6.98-7.05 (m, 2H, ArH), 7.28-7.30 (m,

2H, ArH). Anal. Calcd for ($C_{14}H_{19}FN_20$): C 67.18, H 7.65, N 11.19. Found: C 66.78, H 7.25, N 10.79.

1-[4-[(4-fluorophenyl)methyl]piperazin-1-yl]-2-methylpropan-1-one (11) CAS Number: 1090613-20-9. Yield: 53%. Oily residue. ^{1}H-NMR ($CDCl_3$) (δ): 1.12 (d, 6H, $2CH_3$, J= 6.5), 2.39-2.43 (m, 4H, CH_2), 2.73-2.82 (m, 1H, CH), 3.48-3.50 (m, 4H, CH_2), 3.63-3.65 (m, 2H, CH_2), 6.98-7.04 (m, 2H, ArH), 7.28-7.31 (m, 2H, ArH). Anal. Calcd for ($C_{15}H_{21}FN_2O$): C 68.16, H 8.01, N 10.6. Found: C 68.06, H 7.91, N 10.5.

[4-[(4-Fluorophenyl)methyl]piperazin-1-yl]-phenyl-methanone (12) CAS Number: 439846-67-0. Yield: 16%. m.p. 78-80°C. ^{1}H-NMR ($CDCl_3$) (δ): 1.71 (s, 1H), 2.36 (m, 2H, CH_2), 2.50 (m, 2H, CH_2), 3.42 (m, 2H, CH_2), 3.49 (s, 2H, CH_2), 3.78 (m, 1H), 6.97-7.00 (m, 2H, ArH), 7.25-7.28 (m, 2H, ArH), 7.39 (s, 5H, ArH). Anal. Calcd for ($C_{18}H_{19}FN_2O$) C 72.46, H 6.42, N 9.39. Found: C 72.06, H 6.02, N 8.89.

General procedure to synthesize [4-(4-fluorobenzyl)piperazin-1-yl]methanone derivatives (13-21). To a solution of 1-(4-fluorobenzyl)piperazine (**8**) (0.5mmol) in CH_2Cl_2 (2mL) the N,N-diisopropylethylamine (0.75mmol) and the suitable benzoyl chloride (0.5mmol) were added. The reaction was stirred at room temperature for 5h for compounds **19-21** (Pathway A). Instead, to obtain compounds **13-18** (Pathway B) the reaction was carried out under microwave irradiation 10 min, 50°C, 200 Psi. After turning off the reaction by addition of CH_3OH (2mL), water was added and the mixture was extracted with CH_2Cl_2 (3x5 mL). The obtained organic phase was washed many times with brine (3x5mL) and was dried with anhydrous Na_2SO_4. The solvent was removed under reduced pressure and the final products **13-18** were purified by crystallization with Et_2O.

The registered CAS numbers have been already assigned to compounds **13-21**, for which detailed synthetic procedures, chemical properties and structural characterization are not available in literature.

[4-(4-Fluorobenzyl)piperazin-1-yl](2-fluorophenyl)methanone (13) CAS Number: 444907-73-7. Yield 34%. m.p 78-79°C. ^{1}H-NMR ($CDCl_3$), (δ): 2.40-2.54 (m, 4H), 3.35 (bs, 2H), 3.52 (bs, 2H),

3.83 (bs, 2H, CH_2), 7.00-7.40 (m, 8H, ArH). Anal. Calcd for: ($C_{18}H_{18}F_2N_2O$) C 68.34, H 5.74, N 8.86. Found: C 68.14, H 5.54, N 8.66.

[4-(4-Fluorobenzyl)piperazin-1-yl](3-fluorophenyl)methanone (14) CAS Number: 423739-56-4. Yield 43%. Oily residue. ^{1}H-NMR ($CDCl_3$), (δ): 2.31-2.46 (m, 4H), 3.35-3.44 (m, 4H), 3.71 (bs, 2H), 3.83 (bs, 2H, CH_2), 6.92-7.10 (m, 4H,ArH), 7.20-7.31 (m, 4H,ArH). Anal. Calcd for: ($C_{18}H_{18}F_2N_2O$) C 68.34, H 5.74, N 8.86. Found: C 68.24, H 5.64, N 8.76.

[4-(4-Fluorobenzyl)piperazin-1-yl](4-fluorophenyl)methanone (15) CAS Number: 423748-97-4. Yield 46%. m.p. 112-113°C. ^{1}H-NMR ($CDCl_3$) (δ): 1.25 (s, 1H, CH_2), 1.59 (m, 3H, CH_2), 2.40 (m, 2H, CH_2), 3.50 (m, 3H, CH_2), 3.75 (m, 1H, CH_2), 6.98-7.12 (m, 4H, ArH), 7.26-7.43 (m, 4H, ArH); Anal. Calcd for: ($C_{18}H_{18}F_2N_2O$) C 68.34, H 5.74, N 8.86. Found: C 68.74, H 6.14, N 9.26.

[4-(4-Fluorobenzyl)piperazin-1-yl](2-methylphenyl)methanone (16) CAS Number: 945203-73-6. Yield 56%. m.p. 72-73°C. ^{1}H-NMR ($CDCl_3$) (δ): 1.74 (m, 1H, CH_2), 2.24-2.33 (m, 3H, CH_3), 2.51-2.53 (m, 2H, CH_2), 3.22-3.25 (m, 2H, CH_2), 3.48 (s, 2H, CH_2), 3.82-3.84 (m, 1H, CH_2), 6.97-7.00 (m, 2H, ArH), 7.13-7.33 (m, 6H, ArH). Anal. Calcd for: ($C_{19}H_{21}FN_2O$) C 73.05, H 6.78, N 8.97. Found: C 73.15, H 6.88, 9.07.

[4-(4-Fluorobenzyl)piperazin-1-yl](3-methylphenyl)methanone (17) CAS Number: 945107-54-0. Yield 80%. Oily residue. ^{1}H-NMR ($CDCl_3$) (δ): 2.28-2.49 (m, 3H, CH_3; 4H, CH_2), 3.43-3.77 (m, 6H, CH_2), 6.98-7.04 (m, 4H, ArH), 7.17-7.25 (m, 4H, ArH). Anal. Calcd for: ($C_{19}H_{21}FN_2O$) C 73.05, H 6.78, N 8.97. Found: C 73.14, H 6.87, 9.06.

[4-(4-Fluorobenzyl)piperazin-1-yl](4-methylphenyl)methanone (18) CAS Number: 439846-95-4. Yield 60%. m.p. 114-115°C. ^{1}H-NMR ($CDCl_3$) (δ): 1.70 (s, 1H, CH_2), 2.37 (s, 3H, CH_3), 2.40-2.46 (m, 4H, CH_2), 3.49 (m, 4H, CH_2), 3.75 (m, 1H, CH_2), 6.97-7.04 (m, 2H, ArH), 7.20-7.31 (m, 6H, ArH). Anal. Calcd for: ($C_{19}H_{21}FN_2O$) C 73.05, H 6.78, N 8.97. Found: C 73.25, H 6.98, N 9.17.

[4-(4-Fluorobenzyl)piperazin-1-yl](2-methoxyphenyl)methanone (19) CAS Number: 510718-70-4. Yield 40%. m.p. 78-79°C. ^{1}H-NMR ($CDCl_3$) (δ): 1.62 (m, 1H, CH_2), 2.26-2.54 (m, 4H, CH_2), 3.24-3.26 (m, 2H, CH_2), 3.48 (s, 2H, CH_2), 3.82 (m, 3H, OCH_3; 1H, CH_2), 6.88-7.03 (m, 4H, ArH),

7.22-7.36 (m, 4H, ArH). Anal. Calcd for: ($C_{19}H_{21}FN_2O_2$) C 69.49, H 6.45, N 8.53. Found: C 69.29, H 6.25, N 8.33.

[4-(4-Fluorobenzyl)piperazin-1-yl](3-methoxyphenyl)methanone (20) CAS Number: 462099-41-8. Yield 60%. Oily residue. ^{1}H-NMR ($CDCl_3$) (δ): 2.56 (m, 4H, CH_2), 3.61 (m, 4H, CH_2), 3.82 (m, 3H, OCH_3; 2H, CH_2), 6.93-7.03 (m, 4H, ArH), 7.30-7.32 (m, 4H, ArH). Anal. Calcd for: ($C_{19}H_{21}FN_2O_2$) C 69.49, H 6.45, N 8.53. Found: C 69.28, H 6.24, N 8.32.

[4-(4-Fluorobenzyl)piperazin-1-yl](4-methoxyphenyl)methanone (21) CAS Number: 462096-09-9. Yield 67%. m.p. 120-121°C. ^{1}H-NMR ($CDCl_3$) (δ):1.64 (m, 1H, CH_2), 2.44 (m, 4H, CH_2), 3.47-3.58 (m, 4H, CH_2), 4.11 (m, 3H, OCH_3; 1H, CH_2), 6.88-7.03 (m, 4H, ArH), 7.26-7.40 (m, 4H, ArH). Anal. Calcd for: ($C_{19}H_{21}FN_2O_2$) C 69.49, H 6.45, N 8.53. Found: C 69.79, H 6.75, N 8.83.

General procedure to synthetize 4-(4-fluorobenzyl)piperazin-1-yl](hydroxyphenyl)methanone derivatives (22-24). To a solution of the suitable derivatives **19-21** (0.4mmol) in CH_2Cl_2 (3mL) the BBr_3 (6mmol) was added at 0°C under nitrogen atmosphere. The reaction mixture was stirred for 24h at room temperature, then a small amount of CH_3OH (1.5mL) was added at 0°C.[31] The solvent was removed at reduced pressure and the obtained residue was extracted with EtOAc (3x5mL). The organic phase thus obtained was washed with a saturated solution of $NaHCO_3$ (3x5mL) and subsequently was dried with anhydrous Na_2SO_4. The solvent was removed at reduced pressure and the final products **22-24** were purified by crystallization with CH_3OH.

[4-(4-Fluorobenzyl)piperazin-1-yl](2-hydroxyphenyl)methanone (22) Yield 50%. m.p. 167-169°C . ^{1}H-NMR ($CDCl_3$) (δ): 1.60 (m, 2H, CH_2), 2.48-2.49 (m, 2H, CH_2), 3.52 (s, 2H, CH_2), 3.74-3.82 (m, 4H, CH_2), 6.81-7.05 (m, 4H, ArH), 7.30-7.36 (m, 4H, ArH), 9.63 (s, 1H, OH). Anal. Calcd for: ($C_{18}H_{19}FN_2O_2$) C 68.77, H 6.09, N 8.91. Found: C 68.97, H 6.29, N 9.11.

[4-(4-Fluorobenzyl)piperazin-1-yl](3-hydroxyphenyl)methanone (23) Yield 57%. m.p. 175-177°C. ^{1}H-NMR ($CDCl_3$) (δ): 1.69 (m, 2H, CH_2), 2.36-2.51 (m, 3H, CH_2), 3.43-3.49 (m, 4H, CH_2), 3.78-3.81 (m, 1H, CH_2), 6.80-6.83 (m, 2H, ArH), 6.95-7.04 (m, 2H, ArH), 7.25-7.30 (m, 4H, ArH),

7.54 (bs, 1H, OH). Anal. Calcd for: ($C_{18}H_{19}FN_2O_2$) C 68.77, H 6.09, N 8.91. Found: C 68.89, H 6.21, N 9.03.

[4-(4-Fluorobenzyl)piperazin-1-yl](4-hydroxyphenyl)methanone (24) Yield 70%. m.p. 170-172°C. ^{1}H-NMR ($CDCl_3$), (δ): 1.65 (m, 4H, $2CH_2$), 2.45 (m, 2H, CH_2), 3.50-3.83 (m, 4H, CH_2), 6.73.6.76 (m, 2H, ArH), 6.98-7.04 (m, 2H, ArH), 7.24-7.30 (m, 4H, ArH). Anal. Calcd for: ($C_{18}H_{19}FN_2O_2$) C 68.77, H 6.09, N 8.91; Found: C 68.87, H 6.19, N 9.01.

Crystallization and data collection. TyBm crystals were prepared as described previously.[15] Mature crystals were soaked overnight with 1 µl of 5 mM $CuSO_4$ in 25% PEG 8K and 1 µl of 10 mM inhibitor ligands dissolved in 50% DMSO in distilled water. X-ray diffraction data was collected at the European Synchrotron Radiation Facility, Grenoble, France, at beamline ID 29. All data were indexed, integrated, scaled and merged using Mosflm and Scala.[10] The structure of TyBm with the bound inhibitor was solved by molecular replacement using Phaser [32] and the coordinates of earlier determined TyBm structure (PDB code 4P6R). Refinement was performed using Phenix [33] and Refmac5, [34, 35] coupled with rounds of manual model building, real-space refinement and structure validation performed using COOT.[36] Data collection, phasing and refinement statistics are presented in **Table 2** and **Table 4**.

Docking analysis. The crystal structure of Agaricus Bisporus Mushroom Tyrosinase in complex with inhibitor tropolone was retrieved from the RCSB Protein Data Bank (PDB code 2Y9X). The ligand and water molecules were discarded and the hydrogens were added to the protein by Discovery Studio 2.5.[10] The ligand structure was constructed using Discovery Studio 2.5.5 and energy minimized using the Smart Minimizer protocol (1000 steps) which combines the Steepest Descent and the Conjugate Gradient methods. CHARMm force field was used for energy minimization steps The minimized ligand was docked in their corresponding proteins by means of Gold Suite 5.0.1. The region of interest used by the Gold program[37] was defined in order to contain the residues within 15 Å from the original position of the ligand in the X-ray structure. The side chains of residues Arg 268 and Phe264 were allowed to rotate according to the internal rotamer

libraries in GOLD Suite 5.0.1. A scaffold constraint (penalty = 10.0) was used to restrict the solutions in which the 4-fluorophenyl fragment was able to close-in its binding pose upon the cocrystal structure of the active portion of inhibitor **1** GoldScore was chosen as fitness function. The standard default settings were used in all calculations and the ligands were submitted to 100 genetic algorithm runs. The "allow early termination" command was deactivated. Results differing by less than 0.75 Å in ligand-all atom RMSD, were clustered together. The conformations with the highest GoldScore fitness values were chosen both for analysis and representation The molecular model of the docked compound was displayed using Pymol software. [38]

Mushroom tyrosinase inhibition assay. Mushroom tyrosinase (EC 1.14.18.1) was purchased from Sigma Chemical Co. (St. Louis, MO, USA). Tyrosinase inhibition was assayed according to the method of Masamoto[39] with minor modifications.[40] Briefly, aliquots (0.05mL) of sample at various concentrations (5 – 300 μM) were mixed with 0.5 mL of L- tyrosine or L-DOPA solution (1.25 mM), 0.9 mL of sodium acetate buffer solution (0.05 M, pH 6.8) and preincubated at 25 °C for 10 min. Then 0.05 mL of an aqueous solution of mushroom tyrosinase (333 U/mL) was added last to the mixture. The linear increase in adsorbance (Abs) at 475 nm was measured after 30 or 5 minutes of incubation time in the reaction mixture containing L-DOPA. The inhibitory activity of samples is expressed as inhibition percentage and calculated as follows:

Inhibition % = [[(A-B)-(C-D)]/A-B]/100

A: Abs acetate buffer and enzyme

B: Abs acetate buffer

C: Abs acetate buffer, test sample and enzyme

D: Abs acetate buffer and test sample

The concentrations leading to 50% activity lost (IC_{50}) were also calculated by interpolation of the dose-response curves. Kojic acid [5-hydroxy-2-(hydroxymethyl)-4H-pyran-4-one], a fungal secondary metabolite used as skin whitening agent, was employed as a positive standard (8 – 35

μM). A spectrophotometer (Shimadzu UV-1601) was used for mushroom tyrosinase inhibition assay and kinetic analysis of the tyrosinase inhibition.

Kinetic analysis of the tyrosinase inhibition. The reaction mixture consisted of four different concentrations of L-DOPA (0.6–5 mM) as substrate and mushroom tyrosinase in acetate buffer (0.05 M, pH 6.8). Three different concentrations of compound **19** (2,4,8 μM) were added to the reaction mixture. Michaelis–Menten constant (Km) and maximal velocity (Vmax) of the tyrosinase were determined by Lineweaver–Burk plots.

ACKNOWLEDGMENTS

This work was supported by Fondo di Ateneo per la Ricerca (PRA grant number ORME09SPNC - Università degli Studi di Messina), the Israel Science Foundation founded by the Israel Academy of Sciences and Humanities, grant number 419/15 and by the Gurwin Fund for Scientific Research. We also acknowledge the Russell-Berrie Nanotechnology Institute (RBNI) at the Technion for supporting this research. This research benefited from use of the Technion Center of Structural Biology facility of the Lorry I. Lokey Center for Life Sciences and Engineering. We thank the staff of the European Synchrotron Radiation Facility (beamline ID 29) for provision of synchrotron radiation facilities and assistance, and Mrs. Cristina Iannello for her contribution in the synthesis of several compounds.

ADDITIONAL INFORMATION

PDB accession numbers: The coordinates and structure factors of TyBm have been deposited in the RCSB PDB under accession code 5OAE (TyBm with bound amide **3**) and 6EI4 (TyBm with bound compound **16**). Authors will release the atomic coordinates and experimental data upon article publication.

ASSOCIATED CONTENT

The Supporting Information is available free of charge on the ACS Publications website a DOI…

Molecular formula strings (XLSX)

AUTHOR INFORMATION

Corresponding Author

Laura De Luca: Dipartimento di Scienze Chimiche, Biologiche, Farmaceutiche e Ambientali (CHIBIOFARAM) Polo Universitario SS. Annunziata, Università di Messina, Viale Annunziata I-98168 Messina, Italy. e-mail: ldeluca@unime.it. Phone 00390906766410

Author Contributions

The manuscript was written through contributions of all authors. All authors have given approval to the final version of the manuscript. ∞S.F. and B.D. contributed equally to this work.

Notes

The authors declare no competing financial interest.

ABBREVIATIONS USED

Tys, Tyrosinases; TyM, Mushroom tyrosinase; TyBm, *Bacillus megaterium* tyrosinase; TyIs, Ty inhibitors; TyH, human tyrosinase; TEA, trimethylamine; THF, Tetrahydrofuran; DMF, Dimethylformamide; MW, Microwave; EDIPA, N,N-Diisopropylethylamine; DCM,

dichloromethane; BBr_3, Boron tribromide, EDG, electron donating groups; EWG, electron withdrawing group; KA, kojic acid; FC, Flash Chromatography; TLC, Thin Layer Chromatography.

REFERENCES

1. Pillaiyar, T.; Manickam, M.; Jung, S. H. Recent development of signaling pathways inhibitors of melanogenesis. *Cell Signal* **2017,** *40*, 99-115.

2. Pillaiyar, T.; Manickam, M.; Namasivayam, V. Skin whitening agents: medicinal chemistry perspective of tyrosinase inhibitors. *J. Enzyme Inhib. Med. Chem.* **2017,** *32*, 403-425.

3. Gunia-Krzyzak, A.; Popiol, J.; Marona, H. Melanogenesis Inhibitors: Strategies for Searching for and Evaluation of Active Compounds. *Curr. Med. Chem.* **2016,** *23*, 3548-3574.

4. Lee, S. Y.; Baek, N.; Nam, T. G. Natural, semisynthetic and synthetic tyrosinase inhibitors. *J. Enzyme Inhib. Med. Chem.* **2016,** *31*, 1-13.

5. Haudecoeur, R.; Carotti, M.; Gouron, A.; Maresca, M.; Buitrago, E.; Hardre, R.; Bergantino, E.; Jamet, H.; Belle, C.; Reglier, M.; Bubacco, L.; Boumendjel, A. 2-Hydroxypyridine-N-oxide-Embedded Aurones as Potent Human Tyrosinase Inhibitors. *ACS Med. Chem. Lett.* **2017,** *8*, 55-60.

6. Mann, T.; Gerwat, W.; Batzer, J.; Eggers, K.; Scherner, C.; Wenck, H.; Stab, F.; Hearing, V. J.; Rohm, K. H.; Kolbe, L. Inhibition of Human Tyrosinase Requires Molecular Motifs Distinctively Different from Mushroom Tyrosinase. *J Invest Dermatol,* **2018** *in press 10.1016/j.jid.2018.01.019*

7. Favre, E.; Daina, A.; Carrupt, P. A.; Nurisso, A. Modeling the met form of human tyrosinase: a refined and hydrated pocket for antagonist design. *Chem. Biol. Drug. Des.* **2014,** *84*, 206-215.

8. Lai, X.; Wichers, H. J.; Soler-Lopez, M.; Dijkstra, B. W. Structure of Human Tyrosinase Related Protein 1 Reveals a Binuclear Zinc Active Site Important for Melanogenesis. *Angew. Chem. Int. Ed. Engl.* **2017,** *56*, 9812-9815.

9. Haudecoeur, R.; Gouron, A.; Dubois, C.; Jamet, H.; Lightbody, M.; Hardre, R.; Milet, A.; Bergantino, E.; Bubacco, L.; Belle, C.; Reglier, M.; Boumendjel, A. Investigation of binding-site homology between mushroom and bacterial tyrosinases by using aurones as effectors. *Chembiochem* **2014,** *15*, 1325-1333.

10. Leslie, A. G. W. *joint CCP4 + ESF-EAMCB Newsletter on Protein Crystallography* **1992,** *26*.

11. Ferro, S.; Certo, G.; De Luca, L.; Germano, M. P.; Rapisarda, A.; Gitto, R. Searching for indole derivatives as potential mushroom tyrosinase inhibitors. *J. Enzyme Inhib. Med. Chem.* **2016,** *31*, 398-403.

12. Ferro, S.; De Luca, L.; Germano, M. P.; Buemi, M. R.; Ielo, L.; Certo, G.; Kanteev, M.; Fishman, A.; Rapisarda, A.; Gitto, R. Chemical exploration of 4-(4-fluorobenzyl)piperidine fragment for the development of new tyrosinase inhibitors. *Eur. J. Med. Chem.* **2017,** *125*, 992-1001.

13. Jones, G.; Willett, P.; Glen, R. C.; Leach, A. R.; Taylor, R. Development and validation of a genetic algorithm for flexible docking. *J. Mol. Biol.* **1997,** *267*, 727-748.

14. Gitto, R.; De Luca, L.; Ferro, S.; Buemi, M. R.; Russo, E.; De Sarro, G.; Chisari, M.; Ciranna, L.; Chimirri, A. Synthesis and biological characterization of 3-substituted 1H-indoles as ligands of GluN2B-containing N-methyl-D-aspartate receptors. Part 2. *J. Med. Chem.* **2012,** *55*, 10532-10539.

15. Goldfeder, M.; Kanteev, M.; Isaschar-Ovdat, S.; Adir, N.; Fishman, A. Determination of tyrosinase substrate-binding modes reveals mechanistic differences between type-3 copper proteins. *Nat. Commun.* **2014,** *5*, 4505.

16. Kanteev, M.; Goldfeder, M.; Fishman, A. Structure–function correlations in tyrosinases. *Protein Science* **2015,** *24*, 1360-1369.

17. Deri, B.; Kanteev, M.; Goldfeder, M.; Lecina, D.; Guallar, V.; Adir, N.; Fishman, A. The unravelling of the complex pattern of tyrosinase inhibition. *Sci. Rep.* **2016,** *6*, 34993.

18. Kwong, H. C.; Kumar, C. C.; Mah, S. H.; Chia, T. S.; Quah, C. K.; Loh, Z. H.; Chandraju, S.; Lim, G. K. Novel biphenyl ester derivatives as tyrosinase inhibitors: Synthesis, crystallographic, spectral analysis and molecular docking studies. *PLoS One* **2017,** *12*, e0170117.

19. Goldfeder, M.; Egozy, M.; Shuster Ben-Yosef, V.; Adir, N.; Fishman, A. Changes in tyrosinase specificity by ionic liquids and sodium dodecyl sulfate. *Appl. Microbiol. Biotechnol.* **2013,** *97*, 1953-1961.

20. The PyMOL Molecular Graphics System, Version 2.0 Schrödinger, LLC. .

21. Laskowski, R. A.; Swindells, M. B. LigPlot+: multiple ligand-protein interaction diagrams for drug discovery. *J. Chem. Inf. Model.* **2011,** *51*, 2778-2786.

22. Ismaya, W. T.; Rozeboom, H. J.; Weijn, A.; Mes, J. J.; Fusetti, F.; Wichers, H. J.; Dijkstra, B. W. Crystal structure of Agaricus bisporus mushroom tyrosinase: identity of the tetramer subunits and interaction with tropolone. *Biochemistry* **2011,** *50*, 5477-5486.

23. Hassani, S.; Haghbeen, K.; Fazli, M. Non-specific binding sites help to explain mixed inhibition in mushroom tyrosinase activities. *Eur. J. Med. Chem.* **2016,** *122*, 138-148.

24. Decker, H.; Tuczek, F. The Recent Crystal Structure of Human Tyrosinase Related Protein 1 (HsTYRP1) Solves an Old Problem and Poses a New One. *Angew. Chem. Int. Ed. Engl.* **2017,** *56*, 14352-14354.

25. Chen, W. C.; Tseng, T. S.; Hsiao, N. W.; Lin, Y. L.; Wen, Z. H.; Tsai, C. C.; Lee, Y. C.; Lin, H. H.; Tsai, K. C. Discovery of highly potent tyrosinase inhibitor, T1, with significant anti-melanogenesis ability by zebrafish in vivo assay and computational molecular modeling. *Sci. Rep.* **2015,** *5*, 7995.

26. Dolinska, M. B.; Kovaleva, E.; Backlund, P.; Wingfield, P. T.; Brooks, B. P.; Sergeev, Y. V. Albinism-Causing Mutations in Recombinant Human Tyrosinase Alter Intrinsic Enzymatic Activity. *PLoS One* **2014,** *9*.

27. Park, J.; Boo, Y. C. Isolation of resveratrol from vitis viniferae caulis and its potent inhibition of human tyrosinase. *Evid Based Complement Alternat Med* **2013,** *2013*, 645257.

28. Yoshimori, A.; Oyama, T.; Takahashi, S.; Abe, H.; Kamiya, T.; Abe, T.; Tanuma, S. Structure-activity relationships of the thujaplicins for inhibition of human tyrosinase. *Bioorg Med Chem* **2014,** *22*, 6193-6200.

29. Allen, J.; Bertin, J.; Frost, J.; Vassal, T. 1-(4-Chlorophenyl)-2-[4-(phenylmethyl)piperidin-1-yl]ethanol derivatives, their preparation, and their application in therapeutics as neuroprotective agents. Fr. Demande FR 2672286 . Aug 7, 1992.

30. Schadt, O.; Leibrock, J.; Pruecher, H.; Seyfried, C. Preparation of aminoalkanoylaminobenzoxazoles as excitatory aminoacid antagonists. WO 2003076420, sep 18, 2003.

31. Gitto, R.; De Luca, L.; Ferro, S.; Buemi, M. R.; Russo, E.; De Sarro, G.; Costa, L.; Ciranna, L.; Prezzavento, O.; Arena, E.; Ronsisvalle, S.; Bruno, G.; Chimirri, A. Synthesis and biological characterization

of 3-substituted-1H-indoles as ligands of GluN2B-containing N-methyl-D-aspartate receptors. *J. Med. Chem.* **2011,** *54*, 8702-8706.

32. McCoy, A. J. Solving structures of protein complexes by molecular replacement with Phaser. *Acta Crystall. Section D: Biol. Crystallogr.* **2007,** *63*, 32-41.

33. Adams, P. D.; Afonine, P. V.; Bunkóczi, G.; Chen, V. B.; Davis, I. W.; Echols, N.; Headd, J.; Hung, L.; Kapral, G. J.; Grosse-Kunstleve, R. W. PHENIX: a comprehensive Python-based system for macromolecular structure solution. *Acta Crystallogr. Section D: Biol. Crystallogr.* **2010,** *66*, 213-221.

34. Murshudov, G. N.; Vagin, A. A.; Dodson, E. J. Refinement of macromolecular structures by the maximum-likelihood method. *Acta Crystallogr. Section D: Biol. Crystallogr.* **1997,** *53*, 240-255.

35. Skubak, P.; Murshudov, G. N.; Pannu, N. S. Direct incorporation of experimental phase information in model refinement. *Acta Crystallogr. Section D: Biol. Crystallogr.* **2004,** *60*, 2196-2201.

36. Emsley, P.; Cowtan, K. Coot: model-building tools for molecular graphics. *Acta Crystallogr. Section D: Biol. Crystallogr.* **2004,** *60*, 2126-2132.

37. Jones, G.; Willett, P.; Glen, R. C.; Leach, A. R.; Taylor, R. Development and validation of a genetic algorithm for flexible docking. *J. Mol. Biol.* **1997,** *267*, 727-748.

38. Discovery Studio 2.5.5; Accelrys: San Diego, CA, 2009; http://www.accelrys.com.

39. Masamoto, Y.; Ando, H.; Murata, Y.; Shimoishi, Y.; Tada, M.; Takahata, K. Mushroom tyrosinase inhibitory activity of esculetin isolated from seeds of Euphorbia lathyris L. *Biosci. Biotechnol. Biochem.* **2003,** *67*, 631-634.

40. Germano, M. P.; Cacciola, F.; Donato, P.; Dugo, P.; Certo, G.; D'Angelo, V.; Mondello, L.; Rapisarda, A. Betula pendula leaves: polyphenolic characterization and potential innovative use in skin whitening products. *Fitoterapia* **2012,** *83*, 877-882.

TABLE OF CONTENTS GRAPHIC